

Proceedings of the ASME 2020 15th International Manufacturing Science and Engineering Conference MSEC2020 September 3, 2020, Virtual, Online

MSEC2020-8495

TOP-DOWN PROCESSING TOWARDS ÅNGSTRÖM-THIN TWO-DIMENSIONAL (2D) ELEMENTAL METALS

Md Rubayat-E Tanjil, Stanley Agbakansi, Keegan Phayden Suero, Ossie Douglas, Yunjo Jeong, Zhewen Yin, Wyatt Panaccione, Michael Cai Wang

Department of Mechanical Engineering, University of South Florida, 4202 E. Fowler Avenue, Tampa, FL 33620, USA

ABSTRACT

Two-dimensional (2D) materials have recently garnered significant interest due to their novel and emergent properties. A plethora of 2D materials have been discovered and intensively studied, such as graphene, hexagonal boron nitride, transitionmetal dichalcogenides (TMDCs), and other metallic compound MXenes (nitrides, phosphides, and hydroxides), as well as elemental 2D materials (borophene, germanene, phosphorene, silicene, etc.). Considering the widespread interest in conventional van der Waals 2D materials, two-dimensional metallic nanosheets (2DMNS), a recent addition to the 2D materials family, have exhibited diverse potential spanning optics, electronics, magnetics, catalysis, etc. However, the closepacked, non-layered structure and non-directional, isotropic bonding of metallic materials make it difficult to access metals in their 2D forms, unlike 2D van der Waals materials, which have intrinsically layered structure (strong in-plane bonding in addition to the weak interlayer interaction). Until now, conventional top-down and bottom-up synthesis schemes of these 2DMNS have encountered various limitations such as precursor availability, substrate incompatibility, difficulty of control over thickness and stoichiometry, limited thermal budget, etc. To overcome these manufacturing limitations of 2DMNS, here we report a facile, rapid, large-scale, and costeffective fabrication technique of nanometer-scale copper (Cu) 2DMNS via iterative rolling, folding, and calendering (RFC) that is readily generalizable to other conventional elemental metallic materials. Overall, we successfully show a scalable fabrication technique of 2DMNS.

Keywords: 2D materials, 2D metals, top-down processing

Contact author: mcwang@usf.edu

NOMENCLATURE

T_m melting temperature

S roller gap

 $\begin{array}{ll} P_{avg} & \text{average roller pressure} \\ P_{static} & \text{average static roller pressure} \\ P_{synamic} & \text{average dynamic roller pressure} \end{array}$

1. INTRODUCTION

Nanometer-scale two-dimensional (2D) materials have garnered significant interest due to their emergent physical, chemical, and optical properties that differ from their bulk counterparts [1,2]. In particular, 2D metals possess significant potential towards a broad regime of applications including catalysis, optoelectronics, energy storage, coatings, and separation membranes [3-8]. According to the Mermin-Wagner theorem, the stability of 2D materials has long been debated. However, many 2D materials have since been experimentally realized and have shown outstanding ambient stability owing to their out-of-plane fluctuations and strong in-plane covalency [1]. A plethora of 2D materials have now been discovered and intensively studied, such as graphene, hexagonal boron nitride, elemental 2D materials (borophene, germanene, phosphorene, silicene, etc.), transition-metal dichalcogenides (TMDCs), and other metallic compound MXenes (nitrides, phosphides, and hydroxides) [9].

Various top-down (e.g., mechanical "scotch-tape" or solution-based exfoliation) and bottom-up techniques (e.g., chemical vapor deposition, solvothermal synthesis, etc.) have been well established for the synthesis of 2D materials. Owing to their intrinsic layered structure (strong in-plane bonding in addition to the weak interlayer interaction), isolation of stable

single/few-layer 2D van der Waals sheets from their bulk 3D precursors is readily accessible. However, materials with close-packed, non-layered structures and non-directional, isotropic bonding (e.g., transition metals, metalloids, post-transition metals) do not have an obvious route to access nanometer- or ångström-scale 2D forms.

Elemental metals and their metallic compounds are an integral part of modern conveniences due to their diverse and superlative properties (e.g., ductility/malleability, strength, conductivity, reprocessability/recyclability, etc.) [10]. Metallic materials exhibit unique properties distinct from their 3D bulk counterparts at nanometer length-scales. In particular, 2D metallic nanosheets (2DMNS) can have emergent usefulness for optics, electronics, magnetics, catalysis due to their extremely large surface area to volume ratio and concomitant undercoordination [11].

Currently, various bottom-up, solution-based chemical methods such as hydrothermal and solvothermal synthesis, and templating methods can realize nanometer-thin metallic sheets. Additionally, several top-down approaches such as cathodic exfoliation and mechanical processing have been adopted towards fabricating 2DMNS [12,13]. However, these conventional bottom-up and top-down techniques have limitations such as precursor availability, substrate incompatibility, difficulty of control over thickness and stoichiometry, limited thermal budget, etc.

Recently, a highly versatile rolling scheme of folding and calendering (RFC) technique of 2DMNS fabrication has been developed, motivated by Chinese "qian ceng bing" and French "mille-feuille" [14]. In such RFC technique, two different highpurity metallic sheets are alternatingly stacked (in a vertical superlattice) and folded together (target/primary metal and sacrificial/secondary metal layer). In subsequent repeated rolling, this RFC technique takes advantage of the sequential thickness reduction of both metallic foils towards the nanometer-scale regime. Here, the sacrificial/secondary layer, sandwiched in between the target metallic layers, prevents cold welding of these target metallic layers in the stack (consisting of thousands of alternating metallic layers) during the RFC process [15–17].

Metallic materials have non-directional bonding present in their relatively isotropic lattice structure with a shared 'sea of electrons'. In addition, metals have excellent ductility and malleability. Under compressive loading, the lattice structure undergoes local microscopic plastic deformations, grain boundary distortion, atomic rearrangement, and atomic diffusion through the favorable slip planes. For reference, owing to their denser atomic packing factor (APF), the dislocation gliding is favored in FCC in comparison to BCC metals, making FCC metals more malleable, as exemplified by Cu. Cu is very ductile and malleable and has comparably higher bonding strength relative to other FCC and coinage metals, thus accommodating large deformations without rupturing/dissociation [18].

RFC induced deformation of alternating metallic layers can facilitate the fabrication of a variety of 2DMNS. Moreover, each successive fold increases the number of metallic layers within the gap (i.e., confined space) between the two rollers during the

RFC process. Nominal calculation suggests that the number of metallic (heterogeneous) interfaces is 2^N , where N is the number of folds. For reference, by folding just 10 times, it is possible to generate 1024 alternatingly stacked layers with a concomitant reduction in the layer thicknesses. In addition, during the RFC process, the stacked bimetallic layers require that the chemically dissimilar metals share a similar degree of ductility. If not, under severe rolling deformation, cracks and ruptures occur in the comparatively less ductile metal.

Here, we report a universal and scalable rapid process for efficient, cost-effective and high throughput sub-50 nm Cu 2DMNS from metallic foils through the RFC process, with the goal of accessing ångström-thinness.

2. MATERIALS AND METHODS

2.1 Materials

Here, we have developed a highly versatile top-down approach towards scalable manufacturing of 2DMNS from bulk metallic foil precursors (Figure 1). We have selected Cu as the target/primary material for 2DMNS fabrication due to its intrinsic close-packed FCC crystal structure and high ductility and malleability. Ultra-High Vacuum (UHV) (All Foils, Inc.) Al foils were used as the sacrificial secondary layers, which prevents the cold alloying of adjacent layers of the target/primary metallic layers that would otherwise occur due to the large compressive pressure during the RFC process. The Al and Cu foils, used as precursor materials for 2DMNS fabrication, were 18 µm and 25 µm thick, respectively. A roller press (TMAX-HRP-01 Heat Roll Press Machine, TMAXCN) was used for the RFC process. To mitigate the surface roughness effects from the roller on any non-uniformity induced tearing and cracking of the metal leaves, UHV aluminum foil (25 µm) was annealed and used as an exterior protective sleeve.

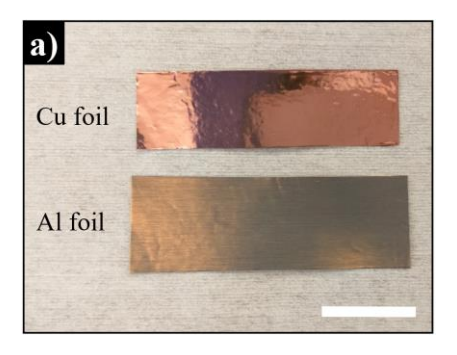


FIGURE 1: Image of commercially procured and annealed a) Copper (Cu) foil, and b) Aluminum (Al) foil. Scale bar is 2 cm.

2.2 Experimental Setup and Procedure

The RFC procedure was performed at ambient conditions (22 °C and ~55% relative humidity) (Figure 2). First, the protective sleeve (i.e., Al foil) was annealed under vacuum condition at 650 °C for 5 hours in a furnace (KJ-1700A, Kejia

Furnace Co. Ltd) to improve ductility and reduce cracking or tearing during RFC procedure. This annealing temperature is just below the melting temperature, T_m of Al (660.3 °C), which promotes stress relaxation, repairing of intrinsic defects, and grain growth. In addition to a 30 min Ar inert gas purge, Ar and H₂ (as reducing gas) gases were used throughout the annealing process of the metal foils. The ramp up and cool down were performed at a rate of 1 °C/min to allow sufficient time for recrystallization and stress relaxation. A similar annealing procedure was performed for the Al foils that were used as sacrificial layers to improve the ductility of the foils for the RFC process. In addition, the primary metal foil (i.e., Cu) was annealed at 1050 °C for 5 hours with a ramp up and cool down rate of 1 °C/min.

Preceding the RFC process, the roller surfaces were degreased and cleaned thoroughly with DI water, acetone and IPA using lint-free cleanroom wipes to remove ambient contaminants (Figure 2). In addition, all metallic foils were cleaned thoroughly with DI water, acetone, and IPA and then dried under a dry nitrogen environment. Here, the annealed Cu foil was placed inside the annealed sacrificial Al foil, and subsequently, the Al/Cu bilayer is manually folded to achieve a sample with lateral dimensions and thickness conducive for effective RFC (Figure 3a). Subsequently, the layered sample was

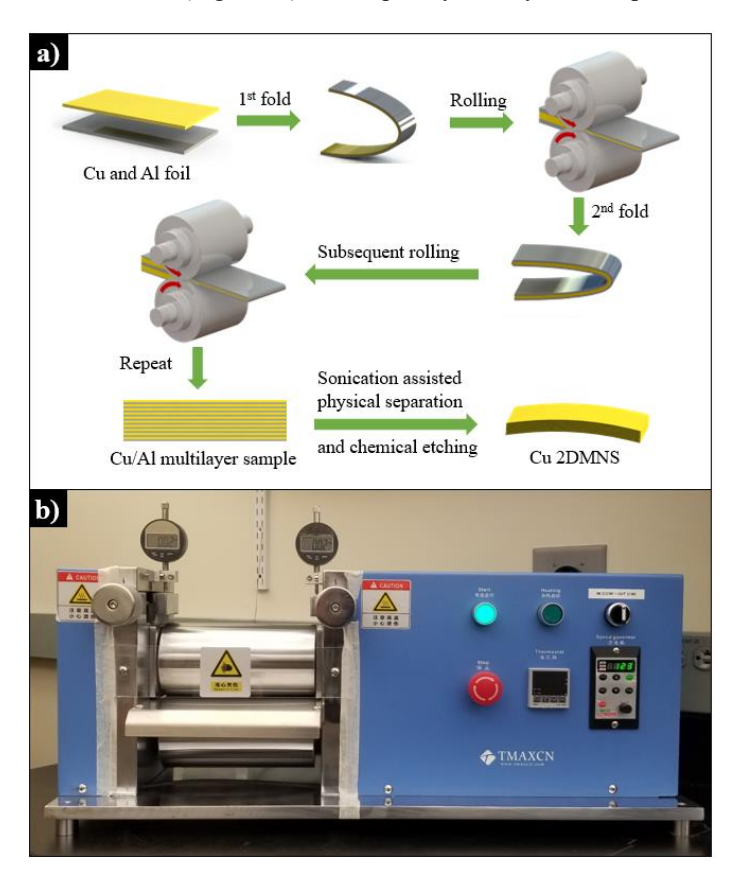


FIGURE 2: a) Schematic of the RFC process, b) Image of the roller used for the experiment.

placed inside the annealed Al protective sleeve and passed through the roller gap. Here, the roller gap, S, is defined as the distance between the two roller surfaces through which the sample passes through during the RFC process (Figure 3b) [19].

Here, the deformation of metals under the rolling procedure is dependent on the rate of thickness reduction as well as the rolling direction. We have experimentally observed that a higher thickness reduction rate makes the Cu/Al sample susceptible to tearing and cracking.

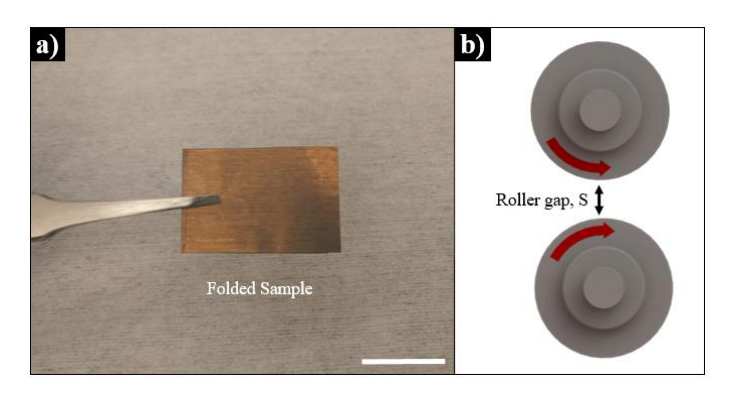


FIGURE 3: a) Cu foil sandwiched within an aluminum leaf and folded once. b) Schematic depicting the roller clearance gap. Scale bar is 3 cm.

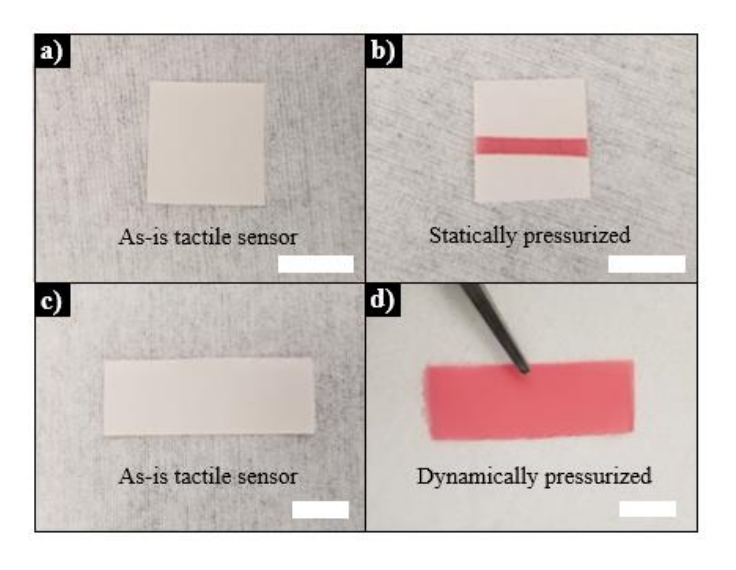


FIGURE 4: Estimation of the pressure regime of the roller via tactile pressure indicating sensor film, which changes color according to the applied localized pressure distribution: a) statically and b) dynamically pressurized sensor film changes color from white to pink. This visual color change provides a pre-estimation of the pressure distribution, which was later accurately measured via software analysis. All scale bars are 1 cm.

We used a rolling speed of 6.60 mm/s, and average pressure, P_{avg} , of 293.2 MPa (i.e., the rolling compressive pressure). We estimated the pressure between the rollers via tactile pressure indicating sensor film (Sensor Products Inc.). As these films are pressurized, the sensor film changes color according to the

applied localized pressure distribution and thus provides an estimation of the pressure history (Figure 4). Two types of pressure measurements were performed: a) static, and b) dynamic. For static pressure measurement, the indicating film was placed in between the rollers, and the roller clearance gap was reduced to the lowest limit. For dynamic pressure measurement, the roller clearance gap was kept at the lowest limit (nominally "0.00 mm") and the sensor film was rolled once. In addition, both the films were analyzed via Topaq® Pressure

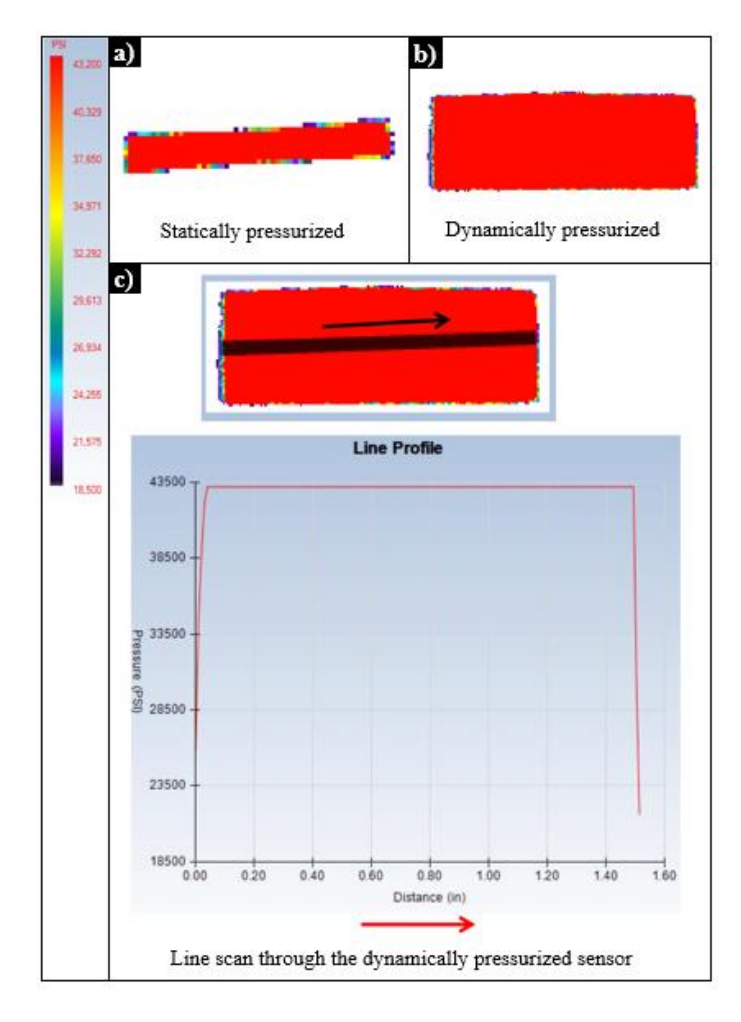


FIGURE 5: Topaq® Pressure Analysis of the sensor films: a) static, b) dynamic test. The contact areas for static and dynamic pressure measurement tests were 32.3 mm², and 548.4 mm², respectively. Here, $P_{\text{static}} = 280.9$ MPa (40,742 psi) and $P_{\text{dynamic}} = 293.2$ MPa (42,524 psi). The maximum pressure for the dynamic pressure test was 297.85 MPa (43,200 psi). Scale bar is shown on the left. c) a line scan through the dynamically pressurized sensor film shows a uniform pressure distribution throughout the sample.

Analysis System (Figure 5). The contact areas for static and dynamic pressure measurement tests were 32.3 mm², and 548.4 mm², respectively. The average pressure for static and dynamic pressure test was, $P_{\text{static}} = 280.9 \text{ MPa} (40,742 \text{ psi})$ and $P_{\text{dynamic}} = 293.2 \text{ MPa} (42,524 \text{ psi})$, respectively. The maximum pressure

for the dynamic pressure test was 297.85 MPa (43,200 psi). A line scan through the dynamically pressurized sensor film shows uniform pressure distribution along the sensor film, thus indicating a uniform pressure distribution throughout the RFC process (Figure 5c).

Here, we employed a thickness reduction rate of 10 μm per each pass for each successive fold of the RFC process. At the initial stage of the rolling for each folding step, the roller gap was kept at 100 μm and gradually decreased (at a rate of 10 $\mu m/roll$) to a final roller gap of 10 μm at the end of the RFC process. Therefore, the entire RFC sequence consists of 10 discrete folding and rolling steps (roller gap decreasing from 100 μm to 10 μm at a constant thickness reduction rate of 10 $\mu m/roll$). Moreover, to mitigate the effects of non-uniform compressive loading across the width of the roller surface, each fold was passed through the roller gap twice by flipping the sample 180° with respect to the sample rolling direction.

After each iteration of folding, the sample is removed from the Al protective sleeve, then folded again and placed inside a newly cleaned and annealed Al sleeve. A new protective sleeve for each folding iteration is necessary because the Al sleeve becomes progressively thinner along with the sample and loses its effectiveness as a mechanically robust sleeve. Overall, the samples are folded 20 times and subsequently rolled using Al foil as the protective sleeve.

2.3 Processing of Cu 2DMNS

After the RFC process, the sample nominally consists of 1048576 (2²⁰, 20 folds during the RFC process) alternating metallic (i.e., Cu and Al) layers. Here, we adopted a novel physical-chemical approach towards etching the Al metallic layers, which leaves isolated, thin Cu metallic nanosheets. First, the Cu/Al multilayer sample was immersed in DI water and vortex mixed for 2 hours. From the rotary motion of the vortex mixer (Four E'S Scientific), the Cu/Al multilayer breaks into smaller (micron-sized) fragments.

Subsequently, the supernatant was extracted to decant the sediment containing micron-sized fragments and then bath sonicated (CO-Z Digital Ultrasonic Cleaner) for 2 hours to physically separate the alternating metallic layers to achieve an aqueous dispersion of Cu and Al 2DMNS. Again, the supernatant was extracted and the Cu and Al 2DMNS sediment were placed in a 2 mole/L NaOH aqueous solution for 24 hours to etch away the Al sacrificial layers.

After the etching process, the Cu 2DMNS were further centrifugally washed using DI water for 20 min and 7 times at 10000 rpm to remove ambient contaminants (BIORIDGE centrifuge), with the supernatant solution discarded after each centrifugation process, and redispersed with fresh DI water to the remaining sediment (i.e., Cu 2DMNS). Subsequently, rigorous vortex mixing for 30 s and bath ultrasonication for 1 min was performed to achieve homogeneous dispersions. Following the washing and dispersion procedure, the solution containing the Cu 2DMNS was drop-casted onto polished Si wafers and vacuum dried for characterization. Here, the Si wafer was

precleaned using piranha solution (sulfuric acid, H_2SO_4 : hydrogen peroxide, $H_2O_2 = 3:1$) and via oxygen plasma (under 100 sccm O_2 for 10 min using Plasma-Therm Reactive Ion Etching, RIE).

3. RESULTS AND DISCUSSION

To understand the effect of rolling induced deformation on the final morphology and thickness of the 2DMNS, we performed optical and electron microscopy characterization of 2DMNS in addition to complementary multi-modal AFM. Hitachi S-800 and Hitachi SU70 scanning electron microscopes (SEM) were used for characterizing the surface morphology of the as-procured metallic foils and synthesized 2DMNS. The SEM images of the as-procured Cu and Al foil demonstrate the surface morphology (Figure 6). In addition, energy-dispersive X-ray spectra (EDS) exhibits the absence of any spurious components in the metallic foils.

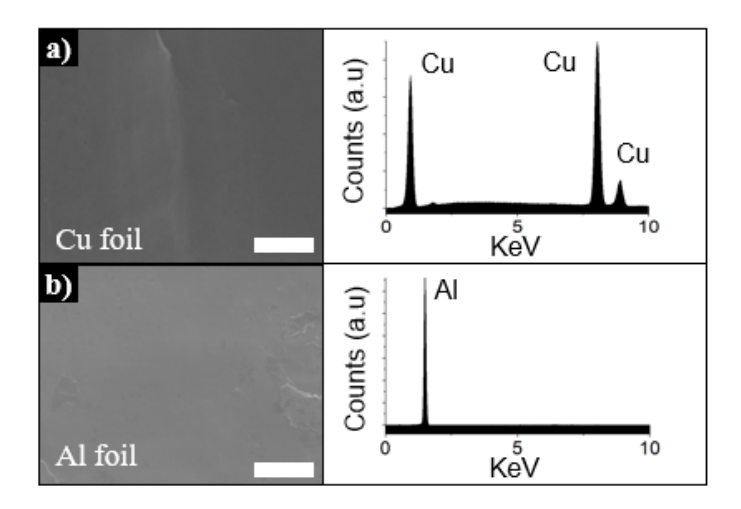


FIGURE 6: SEM images and EDS spectrum of as-procured a) Cu foil, and b) Al foil. EDS demonstrates the absence of any spurious components in the metallic foils. All scale bars shown are 1 μ m.

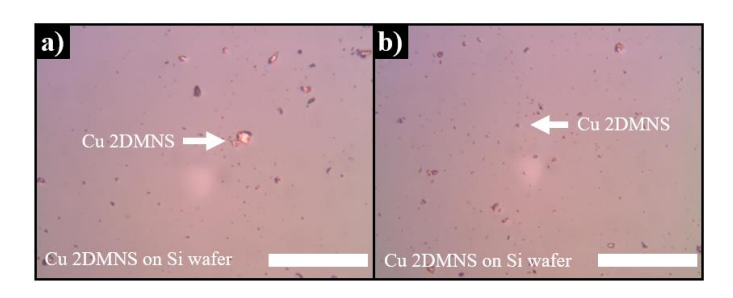


FIGURE 7: a), b) Optical image of Cu 2DMNS vacuum dried on Si wafer. All scale bars shown are 50 μm.

The centrifugal washing protocol of the 2DMNS removed most of the ambient contaminants, as can be seen from the optical images of the as-synthesized and washed Cu 2DMNS (Figure 7).

After the vacuum drying process, isolated Cu 2DMNS are seen to be randomly dispersed on Si wafer (Figure 7, 8). A slight degree of folding can be observed on Cu 2DMNS edges, which might have been generated due to 1) thinner profile along the edge compared to the central area of the 2DMNS, and 2) water evaporation during the drying process (Figure 8). The surface morphology of the Cu 2DMNS appears overwhelmingly smooth, although, some Cu 2DMNS exhibited rough morphology.

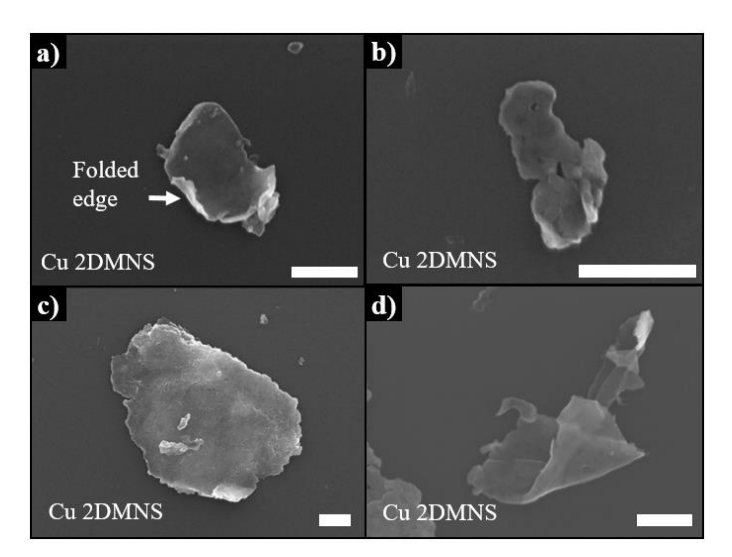


FIGURE 8: a-d) SEM images of Cu 2DMNS. The folded edges of the 2DMNS may have been generated from the thinness and the water evaporation during the drying process. All scale bars shown are 500 nm.

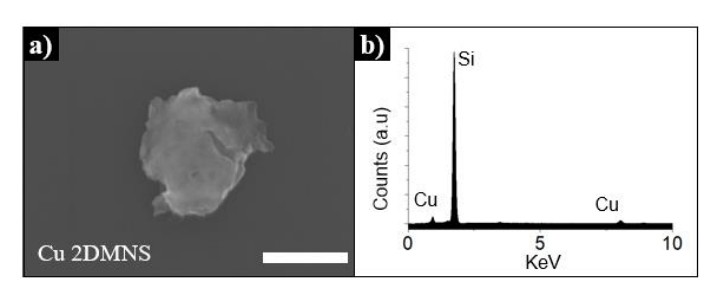


FIGURE 9: Figure showing the a) SEM image and b) EDS spectrum of Cu 2DMNS. EDS spectrum suggests that there was no cold alloying between Cu and Al during the RFC process and physical/chemical separation was successful. Scale bar shown is 500 nm.

The Cu 2DMNS were mono-elemental, with no presence of any intermetallic compound or alloy formation (i.e., cold alloying with Al) due to the RFC process. In addition, the EDS characterization (Figure 9a, and 9b) proves that bath sonication assisted physical separation and etching successfully removed the sacrificial Al layer leaving isolated Cu 2DMNS.

Here, the Cu 2DMNS were characterized by the atomic force microscopy (AFM) using AFM Dimension 3100 to determine their thickness. We have successfully fabricated sub-50 nm metallic nanosheets with lateral dimensions ranging from 100 nm up to micron-scale (Figure 10).

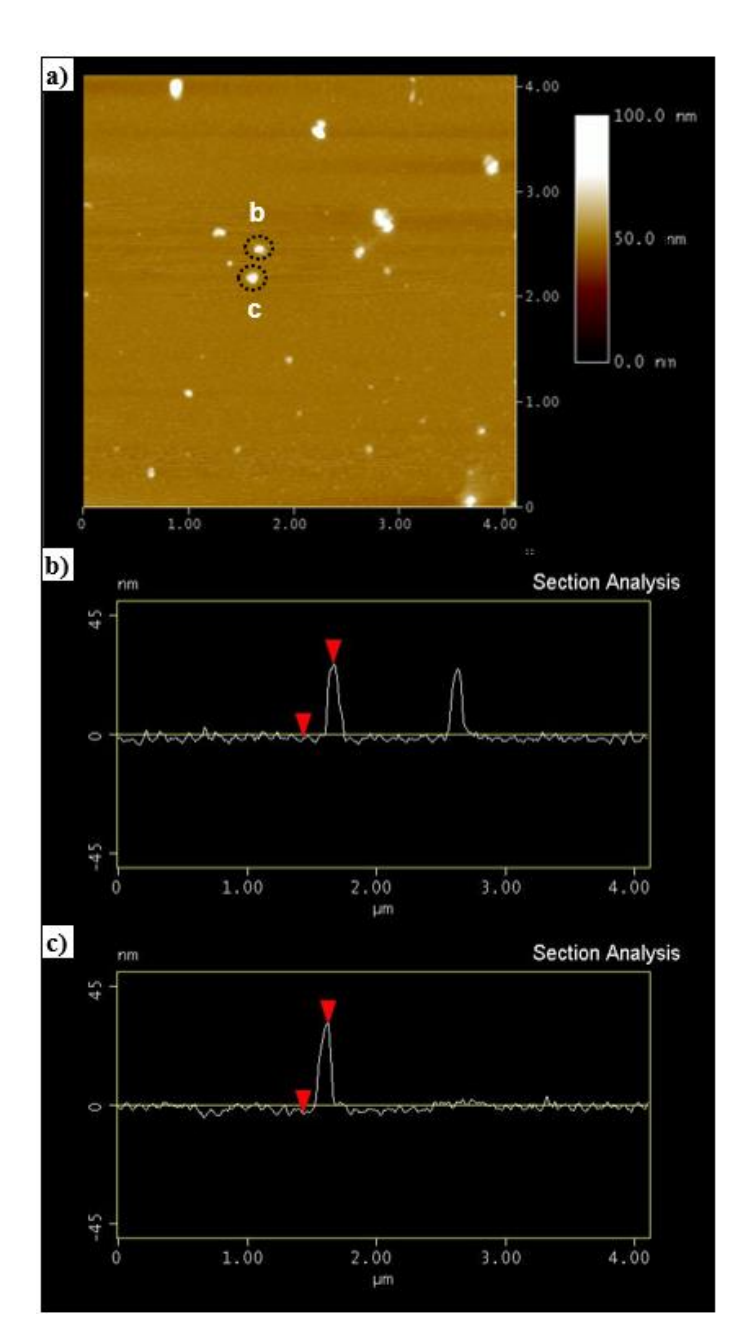


FIGURE 10: a) AFM image of Cu 2DMNS. Two Cu 2DMNS flakes are black circled and indicated as b and c. The thicknesses of the 2DMNS marked by black circles are b) 27.7 nm, and c) 33.8 nm. Scale bar is 100 nm.

4. CONCLUSION

In conclusion, we have successfully demonstrated a scalable and generalizable fabrication technique of 2DMNS using an iterative, rolling, folding, and calendaring (RFC) process. The physical/chemical separation assisted RFC process can be easily generalizable to other conventional metals while maintaining the appropriate purification (washing) protocols to facilitate 2DMNS fabrication and isolation.

ACKNOWLEDGMENTS

This research was supported by USF New Researcher Grant (NRG), USF Nexus Initiative Award, and the USF Research and Innovation Strategic Investment Pool. The authors acknowledge insightful discussions regarding the chemical etching procedures with Emily Phan, assistance with characterization by Dr. Yusuf Emirov of Nanotechnology Research and Education Center (NREC), and the support of Ausmita Sarker. In addition, we acknowledge the contribution of Sensor Product Inc. for assistance with Topaq® Pressure Analysis. This work was partially supported by the National Science Foundation CAREER Award under Grant No. CMMI-1944638.

REFERENCES

- Novoselov, K. S., Geim, A. K., Morozov, S. V, Jiang, D., Zhang, Y., Dubonos, S. V, Grigorieva, I. V, Firsov, A. A., Katsnelson, M. I., Geim, A. K., and Novoselov, K. S., 2004, "Electric Field Effect in Atomically Thin Carbon Films.," Science, 306(5696), pp. 666–9.
- [2] Novoselov, K. S., Jiang, D., Schedin, F., Booth, T. J., Khotkevich, V. V., Morozov, S. V., and Geim, A. K., 2005, "Two-Dimensional Atomic Crystals," Proceedings of the National Academy of Sciences of the United States of America, 102(30), pp. 10451–10453.
- [3] Bonaccorso, F., Colombo, L., Yu, G., Stoller, M., Tozzini, V., Ferrari, A. C., Ruoff, R. S., and Pellegrini, V., 2015, "Graphene, Related Two-Dimensional Crystals, and Hybrid Systems for Energy Conversion and Storage," Science (80), **347**(6217), p. 1246501.
- [4] Gupta, A., Sakthivel, T., and Seal, S., 2015, "Recent Development in 2D Materials beyond Graphene," Progress in Materials Science, 73, pp. 44–126.
- [5] Tanjil, M. R.-E., Jeong, Y., Yin, Z., Panaccione, W., and Wang, M. C., 2019, "Ångström-Scale, Atomically Thin 2D Materials for Corrosion Mitigation and Passivation," Coatings, 9(2), p. 133.
- [6] Hussain, N., Liang, T., Zhang, Q., Anwar, T., Huang, Y., Lang, J., Huang, K., and Wu, H., 2017, "Ultrathin Bi Nanosheets with Superior Photoluminescence," Small, 13(36), p. 1701349.
- [7] Zhang, F., Wu, N., Zhu, J., Zhao, J., Weng, G., Li, J., and Zhao, J., 2018, "Au@AuAg Yolk-Shell Triangular Nanoplates with Controlled Interior Gap for the Improved Surface-Enhanced Raman Scattering of Rhodamine 6G," Sensors and Actuators B: Chemical, 271, pp. 174–182.
- [8] Cao, Z., Fu, H., Kang, L., Huang, L., Zhai, T., Ma, Y., and Yao, J., 2008, "Rapid Room-Temperature Synthesis of Silver Nanoplates with Tunable in-Plane Surface Plasmon Resonance from Visible to near-IR," Journal of Materials Chemistry, **18**(23), pp. 2673–2678.
- [9] Kang, J., Cao, W., Xie, X., Sarkar, D., Liu, W., and Banerjee, K., 2014, "Graphene and Beyond-Graphene

- 2D Crystals for next-Generation Green Electronics," Micro- and Nanotechnology Sensors, Systems, and Applications VI, SPIE, p. 908305.
- [10] Mridha, S., 2016, "Metallic Materials," Reference Module in Materials Science and Materials Engineering, Elsevier.
- [11] Yonezawa, T., 2018, "Preparation of Metal Nanoparticles and Their Application for Materials," Nanoparticle Technology Handbook, pp. 829–837.
- [12] Pei, Y., Huang, L., Wang, J., Han, L., Li, S., Zhang, S., and Zhang, H., 2019, "Recent Progress in the Synthesis and Applications of 2D Metal Nanosheets," Nanotechnology, **30**(22), p. 222001.
- [13] Ma, Y., Li, B., and Yang, S., 2018, "Ultrathin Two-Dimensional Metallic Nanomaterials," Materials Chemistry Frontiers, 2(3), pp. 456–457.
- [14] Liu, H., Tang, H., Fang, M., Si, W., Zhang, Q., Huang,
 Z., Gu, L., Pan, W., Yao, J., Nan, C., and Wu, H., 2016,
 "2D Metals by Repeated Size Reduction," Advanced
 Materials, 28(37), pp. 8170–8176.
- [15] Liu, Y., Xiong, L., Li, P., Fu, H., Hou, Z., Zhu, L., and Li, W., 2019, "Self-Supported CuO Nanoflake Arrays on Nanoporous Cu Substrate as High-Performance Negative-Electrodes for Lithium-Ion Batteries," Journal of Power Sources, pp. 20–26.
- [16] Gu, J., Li, B., Du, Z., Zhang, C., Zhang, D., and Yang, S., 2017, "Multi-Atomic Layers of Metallic Aluminum for Ultralong Life Lithium Storage with High Volumetric Capacity," Advanced Functional Materials, 27(27), p. 1700840.
- [17] Xu, Y., Huang, K., Ou, G., Tang, H., Wei, H., Zhang, Q., Gong, J., Fang, M., and Wu, H., 2017, "A Facile Fabrication Method for Ultrathin NiO/Ni Nanosheets as a High-Performance Electrocatalyst for the Oxygen Evolution Reaction," RSC Advances, 7(30), pp. 18539–18544.
- [18] Yang, L. M., Frauenheim, T., and Ganz, E., 2016, "Properties of the Free-Standing Two-Dimensional Copper Monolayer," Journal of Nanomaterials, **2016**, pp. 1–6.
- [19] Gabelaya, D. I., and Kabakov, Z. K., 2019, "Optimization of the Gap Parameters of Supporting Rollers of Curvilinear Continuous Casting Machine," Metallurgist, 63(7–8), pp. 823–828.